Testing ALS Visualisation Methods for Detecting Kiln Remains in a Densely Vegetated Area in Japan

Irmela HERZOG, The Rhineland Commission for Archaeological Monuments and Sites, Germany
Michael DONEUS, Department of Prehistoric and Historical Archaeology, University of Vienna, Austria
Maria SHINOTO, Heidelberg University, Germany
Hideyuki HAIJIMA, Nakanihon Air Service, Japan
Naoko NAKAMURA, Kagoshima University, Japan

Abstract: In May 2018, Lidar data was acquired in a densely vegetated test area in southern Japan with the aim of detecting Sue kiln sites, that date back in the 9th century. In the region including the test area, several surveys as well as an excavation recorded evidence of such sites in recent years. As the densely forested, mountainous topography complicates any ground based archaeological investigations, airborne Lidar was considered the method of choice for surveying the area. This is the first study of this kind in Japan. The company that acquired the Lidar data also provided lists of ground points. Initial interpolations and visualisations relied on these lists; later the program SCOP++ was applied for generating digital terrain models based on alternative ground point selection strategies. The results of several approaches for visualising and analysing the Lidar data sets will be presented and discussed. For visualisations, mainly low-cost or free software was applied, including GIS software, the Relief Visualisation Toolbox (RVT), and planlauf/TERRAIN for 3D virtual flights. Additional GIS approaches for analysing the data are presented: (1) contour maps that assist navigation in the field, (2) a density map of ground points allows assessing the reliability of the Lidar visualisations, (3) cross sections are useful for validating the features recognized and measuring their depth or height, and (4) slope maps support delimiting manmade terraces, identifying platforms and are an important input for deductive predictive modelling of Sue kiln sites. The work of mapping probable kiln locations detected in the LiDAR data and verifying these sites by traditional prospection methods is still in progress. Only after reliably identifying a large number of Sue kilns in the test area, approaches such as predictive modelling or machine learning may be applied for locating additional kilns in this region.

Keywords: *ALS—ground point filtering—Lidar visualisation—point density map—slope map—Sue kilns—Japan*

CHNT Reference: Herzog, Irmela; Doneus, Michael; Shinoto, Maria; Haijima, Hideyuki, and Nakamura, Naoko. 2021. Testing ALS Visualisation Methods for Detecting Kiln Remains in a Densely Vegetated Area in Japan. Börner, Wolfgang; Kral-Börner, Christina, and Rohland, Hendrik (eds.), Monumental Computations: Digital Archaeology of Large Urban and Underground Infrastructures. Proceedings of the 24th International Conference on Cultural Heritage and New Technologies, held in Vienna, Austria, November 2019. Heidelberg: Propylaeum.
doi: 10.11588/propylaeum.747.

Introduction

At Nakadake Sanroku, Kagoshima prefecture, southern Japan, remains of Sue pottery kilns dating in the 9th century were first detected in the 1980ies (Fig. 1a). Kiln site clusters for the production of

Sue ware exist all over Japan, Nakadake being the southernmost location. Since 2012, field walking surveys and geophysical prospection as well as an excavation have documented several Sue pottery kilns in the Nakadake region (Nakamura and Yoshimoto, 2015; Nakamura and Shinoto, 2015; Matsusaki, 2018; Shinoto and Nakamura, 2016). These investigations resulted in an estimated number of about 60 kilns in this region, an unexpectedly large number in this remote region.

The Sue kilns were constructed by digging tunnels into the slope of hills. In the Nakadake area, excavation results suggest an approximate tunnel length of 8 m and a width of about 2 m. The maximum height of the vessels found in such tunnels is about 50 cm, thus providing a lower limit for the tunnel height. At the foot of the tunnel, ash heaps contain waste from the firing process. It seems that most of the tunnels collapsed in the course of time resulting in elongated shallow depressions. These remains are hard to detect due to their mostly inconspicuous shape and because of their location in a densely forested, mountainous area (Fig. 1b). Only if the ash heaps were partly destroyed by erosion processes and relocated downhill by heavy rains, the kiln locations could be identified successfully by walking the area. Consequently, the efficiency of traditional methods for identifying kiln locations is rather limited.

a *b*

Fig. 1. a) Location of the study area; b) typical vegetation (© Google Earth; Maria Shinoto).

In this situation, airborne Lidar was considered the method of choice for effectively identifying additional kiln sites. In Japanese archaeology, previous Lidar projects are limited in number and focussed on the measurement of prominent features such as tombs or castle remains (e.g. Akashi, 2010; Fujii et al., 2015); explicit experiments with different filters and visualisations were not included. This new project had to face complex challenges in view of mostly inconspicuous sites in an area that experienced considerable relief change by agricultural use during medieval and early modern times. Further complications are introduced by dense vegetation, steep slopes, and large differences in altitude ranging from 20 to 265 m above sea level in an area of about 0.5 km². In May 2018, Lidar data was acquired using a scanner of type RIEGL VUX-1 UAV on an octocopter (Glyphon Dynamics GD-X8-SP) in a test region covering 0.5 km² (Fig. 2). At least 100 points/m² were recorded with a conservatively estimated horizontal precision of 10 cm on densely covered forest surface.

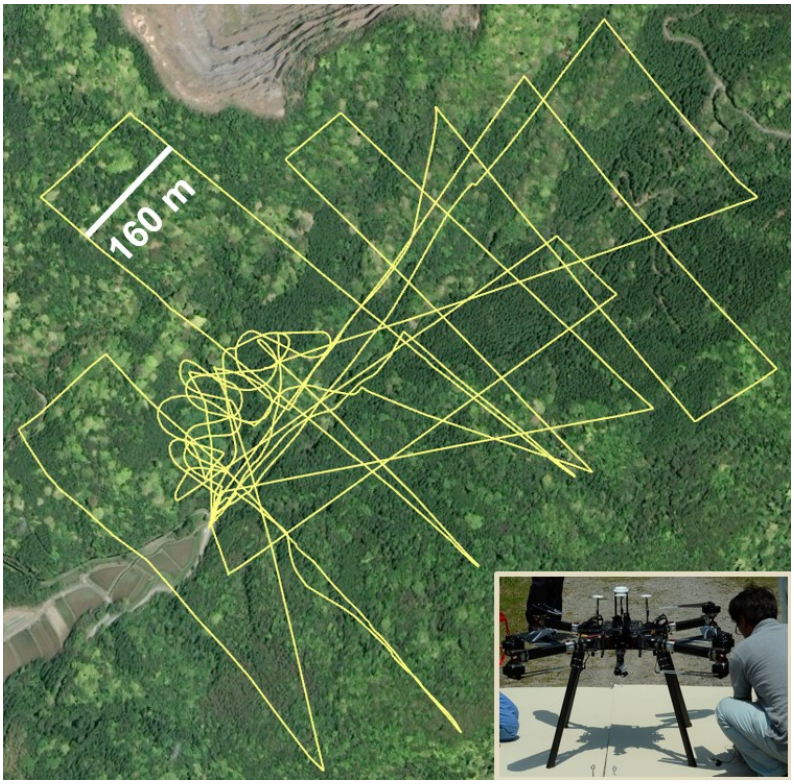

Fig. 2. Itinerary of the UAV flights (yellow) including flights for calibration purposes. Inset image: preparing the UAV (© Google Earth; Maria Shinoto).

Experience from the Rhineland area had shown that sunken roads could be reliably identified in forest areas based on 1 m grid data (Herzog, 2017). Therefore, it seemed more than likely that the laser scanning elevation data of the Japanese study area suffices for detecting kiln sites. However, postprocessing the data turned out to be a challenge. This article will discuss the outcomes including some of the difficulties met when applying the low-cost or free software available for the visualisation of Lidar data. The results of analysing the data by additional GIS approaches are presented: these include contour maps, that assist navigation in the field; a density map of ground points for assessing the reliability of the Lidar visualisations; cross sections, that are useful for validating the features recognized and assessing their depth or height; slope maps, that are an important input for deductive predictive modelling of Sue kiln sites.

Processing the Lidar data

In May 2018, Nakanihon Air Service (NNK) recorded the Lidar data and about one month later, they provided the outcome in four file formats, subdivided into nine tiles, each covering 400 m×300 m (Fig. 3). The file formats and their respective sizes are: LAS (29.4 GB), XYZ (163 MB), GRD (10.7 GB), and TIF (1.2 GB).

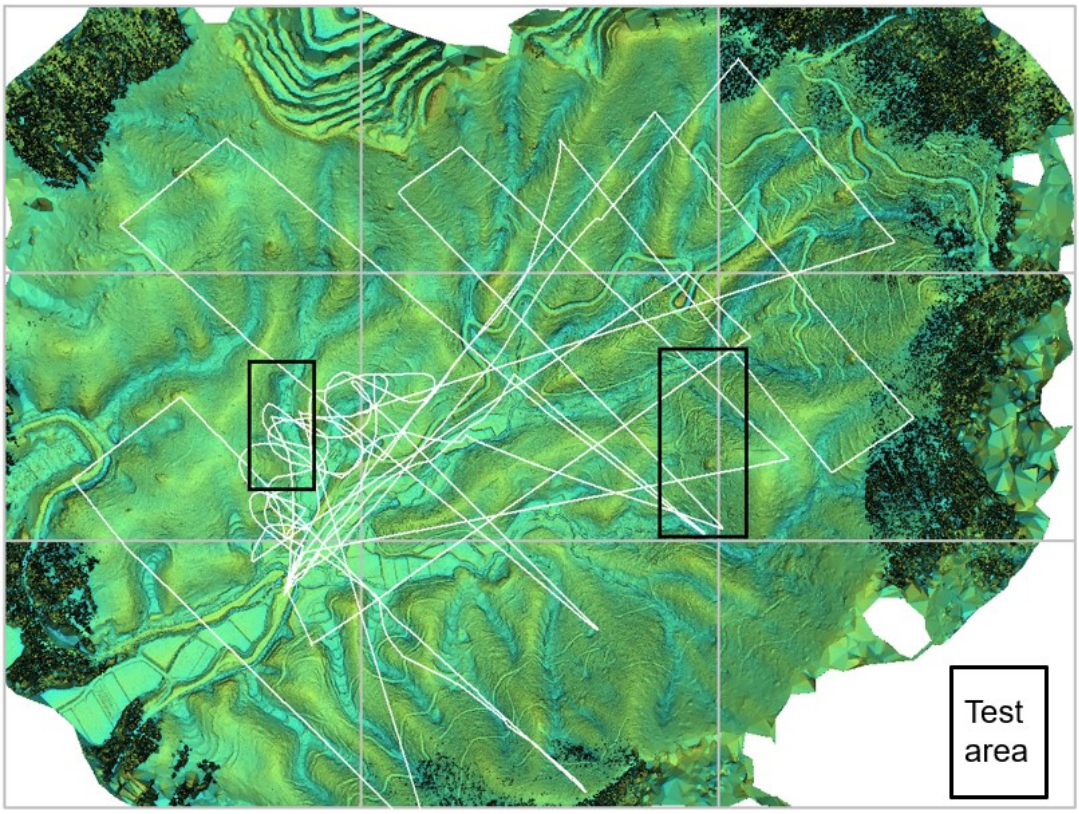

Fig. 3. Visualisation of the Lidar data created by NNK divided into 9 tiles (tile size: 400 m×300 m), UAV itineraries, and test areas (© Nakanihon Air Service; Irmela Herzog).

The LAS file format is an open standard maintained by the American Society for Photogrammetry and Remote Sensing (https://www.asprs.org/divisions-committees/lidar-division/laser-las-file-format-exchange-activities). The binary LAS files contain the 3-dimensional point cloud data recorded during the UAV flights. Each XYZ file is an ASCII list of irregularly distributed 3D points. These points are the results of a filtering process intended to remove all non-ground points from the point cloud. The GRD files are in the Golden Software ASCII Grid file format and store raster data with a cell size of 5 cm. The raster grids were computed by interpolating the XYZ points.

The TIF files present an impressive visualisation in areas covered well by the UAV itineraries (Fig. 3). However, it is difficult to delimit the areas of high reliability. Another issue is the fact that many viewers of these visualisations tend to misinterpret the relief, i.e. the valleys are seen as ridges and vice versa. Moreover, the TIF files do not allow further analysis such as slope calculations or cross sections.

Initially, generating visualisations based on the high resolution ASCII grid files seemed to be the most efficient approach. QGIS was used for converting the GRD files from Golden Software ASCII Grid to ESRI ASCII grid. The latter file format is supported by most GIS software as well as the Relief Visualisation Toolbox (RVT – Kokalj et al., 2013; Kokalj and Somrak, 2019) and the Windows program planlauf/TERRAIN (planlauf GmbH, 2019). Several additional grids were interpolated based on the XYZ data by MapInfo with plugin Vertical Mapper (MIP/VM). The grid with a resolution of 10 cm created by triangulation interpolation will be used for the comparisons presented in the next section.

The software package SCOP++ (Doneus and Briese, 2006; Pfeifer et al., 2001) was applied for processing the LAS files, providing alternative ground point filter results and subsequent interpolations. Due to substantial variations in vegetation density, SCOP++ was run with two different filter strategies:

Strategy 1: Filter settings tweaked for high detail, DTM resolution: 7 cm

While the results are very good in areas with a fairly low vegetation density, in areas with extremely dense vegetation, a considerable number of non-ground points is still clearly visible and this complicates the detection of archaeological features.

Strategy 2: Filter settings adapted to very dense vegetation, DTM resolution: 20 cm

The results of this strategy appear more smooth, and terrain details at a small scale are obscured.

Details on such filter strategies are published in Doneus et al. (2020).

Two test areas were selected for analysing and visualising the Lidar data (Fig. 3). They differ in that the task of analysing test area no. 1 in the western part of the survey area was considered comparatively easy, whereas test area 2 is more of a challenge. Test area 1 is entirely contained in one tile, whereas the data of test area no. 2 was supplied in two different tiles. Most of test area 2 is in higher altitudes than test area 1, and the expectation is that Sue kiln sites are mostly located in low lying parts of this landscape.

Visualisation of the Lidar data

MIP/VM offers routines for creating shaded relief visualisations for DTMs. Identical hill-shading parameters were applied for the MIP/VM interpolated 10 cm grid and the two SCOP++ grids. This allows comparing the outcomes of the different interpolation and filter approaches. Figs. 4 and 5 also show the initial TIF images provided by NNK. The visualisations of test area 1 in Fig. 4 depict a valley with several incised features, some of which seem to overlap.

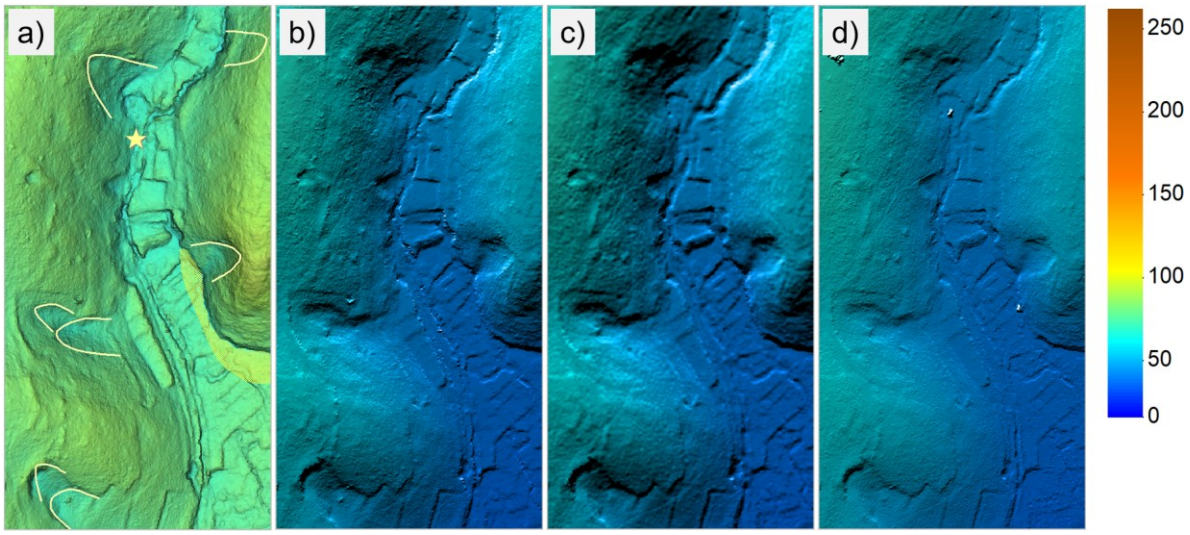

Fig. 4. Visualisation of the Lidar data in test area 1: a) created by NNK, yellow lines delimit potential kilns, find locations are also marked in yellow, b) to d) hill-shading (azimuth=0, inclination=30, contrast=150, brightness=80) created by MIP/VM using the colour profile shown on the right, b) XYZ point interpolation by MIP/VM, c) SCOP++, strategy 2, d) SCOP++ strategy 1 (© NNK, Irmela Herzog, Michael Doneus, and Maria Shinoto).

These typical depressions (delimited by yellow lines in Fig. 4a) were also documented in other valleys where indicators of kilns were found, these indicators include sherds from ash heaps and readings from geomagnetic surveys (Shinoto, 2019a). Although the valley depicted in Fig. 4 had been covered by walking several times since 2012, no kilns were detected before the Lidar data was acquired. Using a map generated from the Lidar data, typical Sue pottery sherd was found in a creek (marked by a yellow star symbol in Fig. 4a), providing evidence that at least one of the kiln site candidates in the upper valley is indeed a kiln site. In the eastern part of the valley depicted in Fig. 4a, the area with the yellow pattern includes find spots of several fragments originating from an ash heap in the incipient stage of erosion, discovered when revisiting the valley.

The legend of Fig. 4 also applies for the test area 2 visualisations b) to d) in Fig. 5. Terraces and paths are clearly visible in all shaded relief images of the DTMs shown in Fig. 5. In the south of test area 2, a valley and some depressions on the slope towards the valley can be detected. At first, one of them was considered as a possible kiln location, but this turned out to be highly unlikely (see below). The depressions were probably created by erosion processes.

Figs. 4 and 5 b) to d) illustrate the differences in the filtering strategies. Fig. 5b) suggests that the DTM derived from the XYZ points includes undergrowth points in densely vegetated areas because the surface is very uneven in some parts that appear fairly smooth in the SCOP++-DTMs. On the other hand, in the XYZ-DTM, no gross errors are evident in the test areas, but both SCOP++ filter results show small spikes indicating non-ground points. In the southern part of Fig. 5, the XYZ-DTM has gaps due to lack of point data, whereas the SCOP++ results show clusters of spikes in these areas.

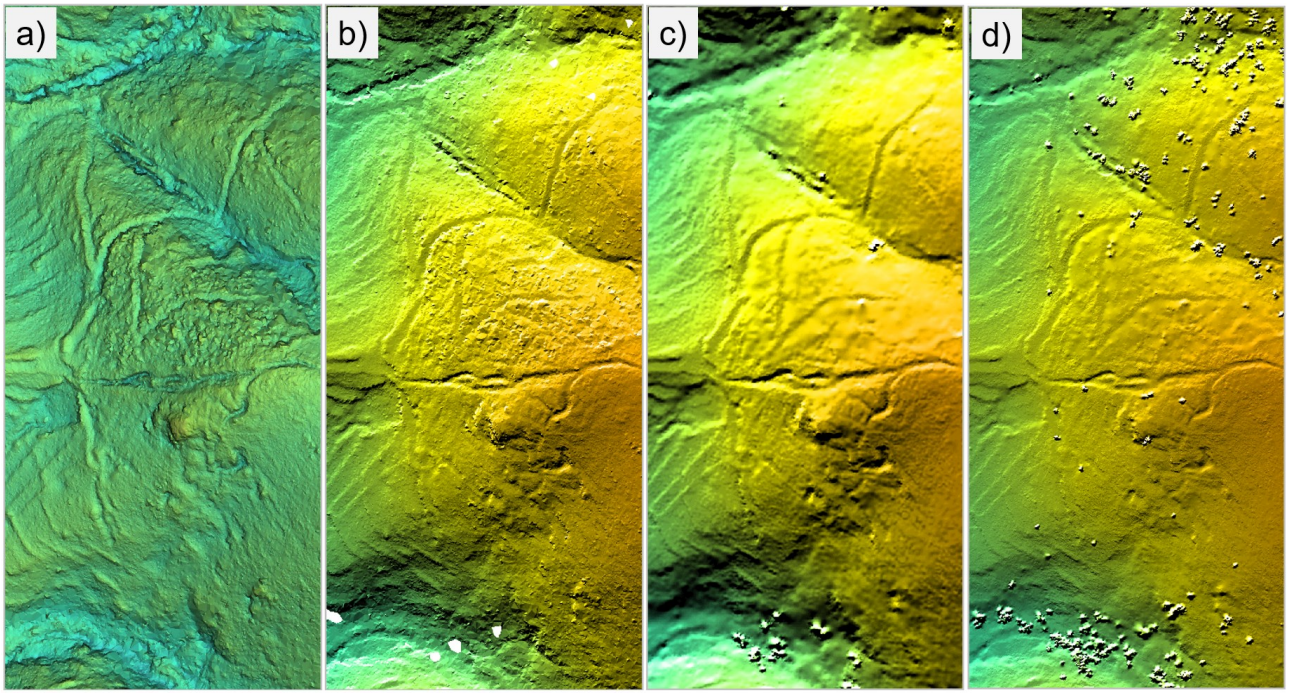

Fig. 5. Visualisation of the Lidar data in test area 2: a), b), c), d) as in Fig. 4 (© NNK, Irmela Herzog, and Michael Doneus).

In the archaeological community additional visualisations of the ALS data are often considered in order to avoid some of the drawbacks of simple hill-shading. A popular alternative visualisation

method is Simple Local Relief Model (SLRM) also known as trend removal. The aim of this approach is to remove the large-scale landscape trend from the DTM so that only local small-scale features remain (Hesse, 2010).

Often, GIS software is able to generate SLRM visualisations. The SLRM computations in Fig. 6 were created by the applying the *Mean(neighbourhod)* and the *Minus Calculus* tool provided by the Sextante toolbox in gvSIG. A neighbourhood radius of 20 pixels was chosen, corresponding to 2 m. For the resulting local relief DTM, an intuitive colour scheme (local depressions are displayed in green and minor earth deposits such as mounds or local ridges are shown in brown) is combined with some hill-shading to enhance readability. This visualisation is very useful for identifying extremely shallow relief features and delimiting features such as platforms, sunken roads, and rice terraces. SLRM avoids the risk of optical illusions inherent in shaded relief images, thus supporting a more accurate mapping of archaeological features in GIS. But some drawbacks are known as well: for larger features local relief elevations are underestimated, features on gradients appear somewhat distorted (Hesse, 2010), and SLRM often produces images showing fake ditches for mounds (Hesse, 2016).

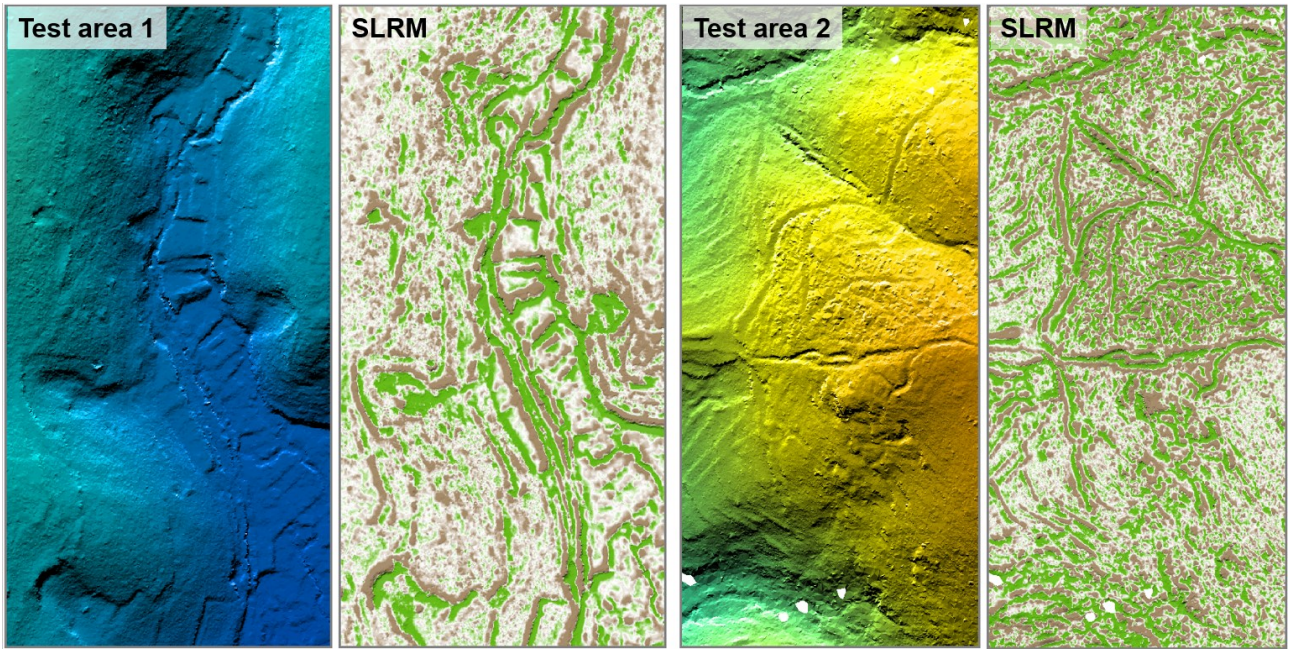

Fig. 6. Hill-shading of test areas 1 and 2 as in Fig. 4b) and 5b) and corresponding SLRM visualisations (© Irmela Herzog).

The user-friendly toolbox RVT offers nine additional methods for visualising elevation grid data beyond simple hill-shading images and SLRM. All desired visualisations can be generated in one run. Version 1.3 of this software was successfully applied for nearly all Lidar grid tiles provided by the Ordnance Survey institution in the Rhineland (Herzog, 2017). For the Rhineland data, hill-shading from multiple directions as well as positive and negative openness were considered the most useful RVT methods. For five of the Lidar data grid tiles in the Japanese study area, all possible visualisation options of RVT 1.3 with default parameters were generated for unchanged elevation and exaggeration factor 5. A selection of the resulting images is presented in Fig. 7. Multiple hill-shade images are the favourite visualisations of many archaeologists, because they deliver an intuitive picture avoiding the drawbacks of single hill-shade images. But directional bias results in horizontal

displacement of features. Therefore, this visualisation is often supplemented by another visualisation such as positive or negative openness. For the two test areas, principal components analysis and anisotropic sky-view-factor provided useful visualisations.

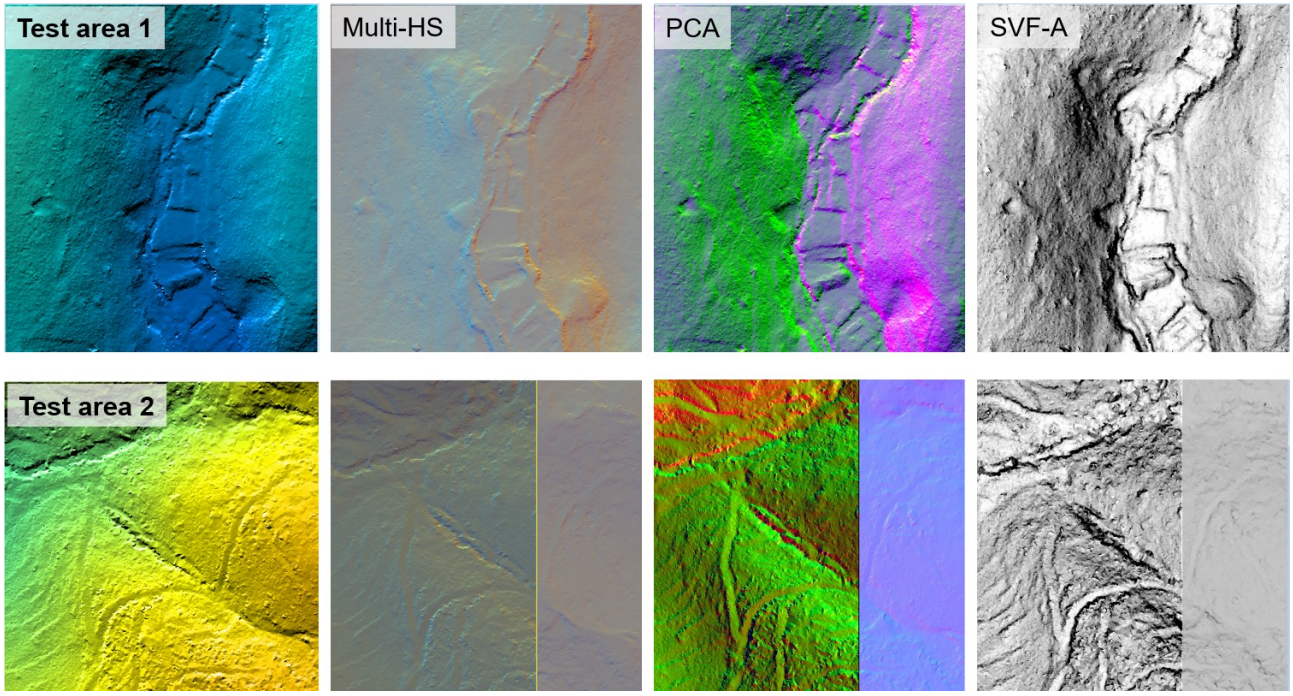

Fig. 7. Hill-shading of the northern parts of test areas 1 and 2 as in Fig. 4b) and 5b) and RVT results (Multi-HS = multi hill-shading; PCA = principal components analysis; SVF-A = anisotropic sky view factor) based on the GRD tiles (© Irmela Herzog).

However, two difficulties were met when working with the RVT toolbox and the tiled data: some of the RVT outcomes based on ESRI ASCII grids derived from the GRD files supplied by NNK or calculated by GIS software were disappointing at first sight. Only after appropriate adjustment of the colour scheme, local features became visible. This issue could be avoided to some extent by converting the DTMs to the GeoTiff file format by QGIS 3.4. Another issue is evident in Fig. 7, which is based on GeoTiff files derived from the GRD files: the results for each tile file depend on the mean local standard deviation of the altitudes. The tile covering the eastern part of test area 2 includes many spiky areas in the east (cf. Fig. 3), therefore mean local variation is high, and the contrast of the visualisation in the western part of the tile is very low.

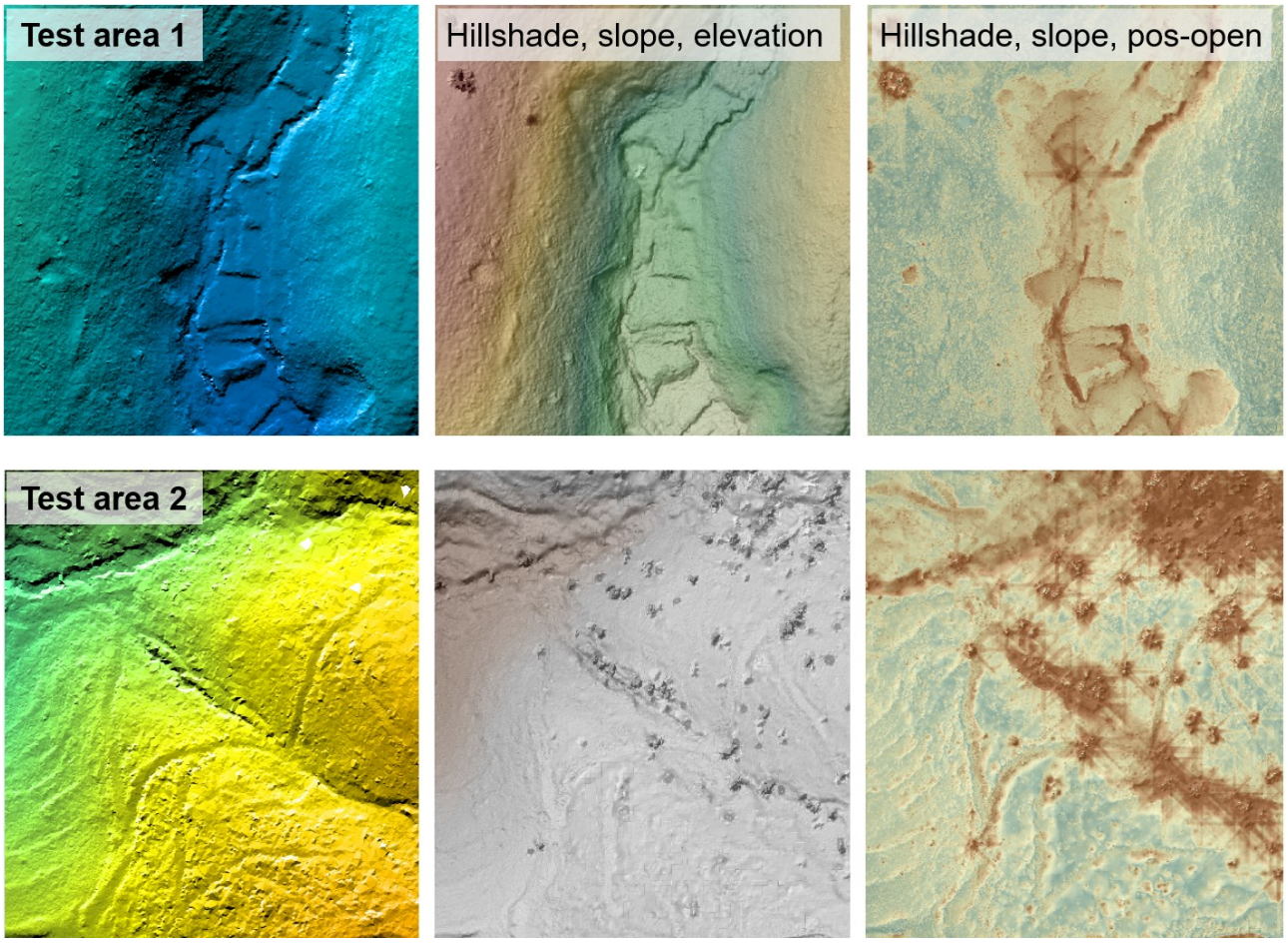

Fig. 8. Left: Hill-shading of the northern parts of test areas 1 and 2 as in Fig. 4b) and 5b). Centre and right: results of blending several visualisations (© Michael Doneus, Irmela Herzog).

The visualisations of the SCOP++ outcome (strategy 1) in Fig. 8 use GIS functions to blend several layers, thus combining a set of visualisations into a single image (see also Kokalj and Somrak, 2019). In the images in the centre, slope, shaded relief and colour-coded heights (focusing on the range between 30 and 140 m above sea level) were combined. The images on the right were generated from shaded relief, slope and positive-openness layers. Considering test area 1, the combined visualisation depicted in the centre of Fig. 8 turned out to be particularly helpful for the archaeologists because some of the details of the probable kiln sites are clearly visible. But in test area 2 with higher elevations, this visualisation lacks contrast. So even with very refined blended images, it might still be necessary to check several visualisation methods or to adjust their parameters in order to unleash the full potential of the Lidar data for detecting archaeological features. In this project, the comparison of several visualisations was also an integral part of preparations for field work targeted at checking possible sites.

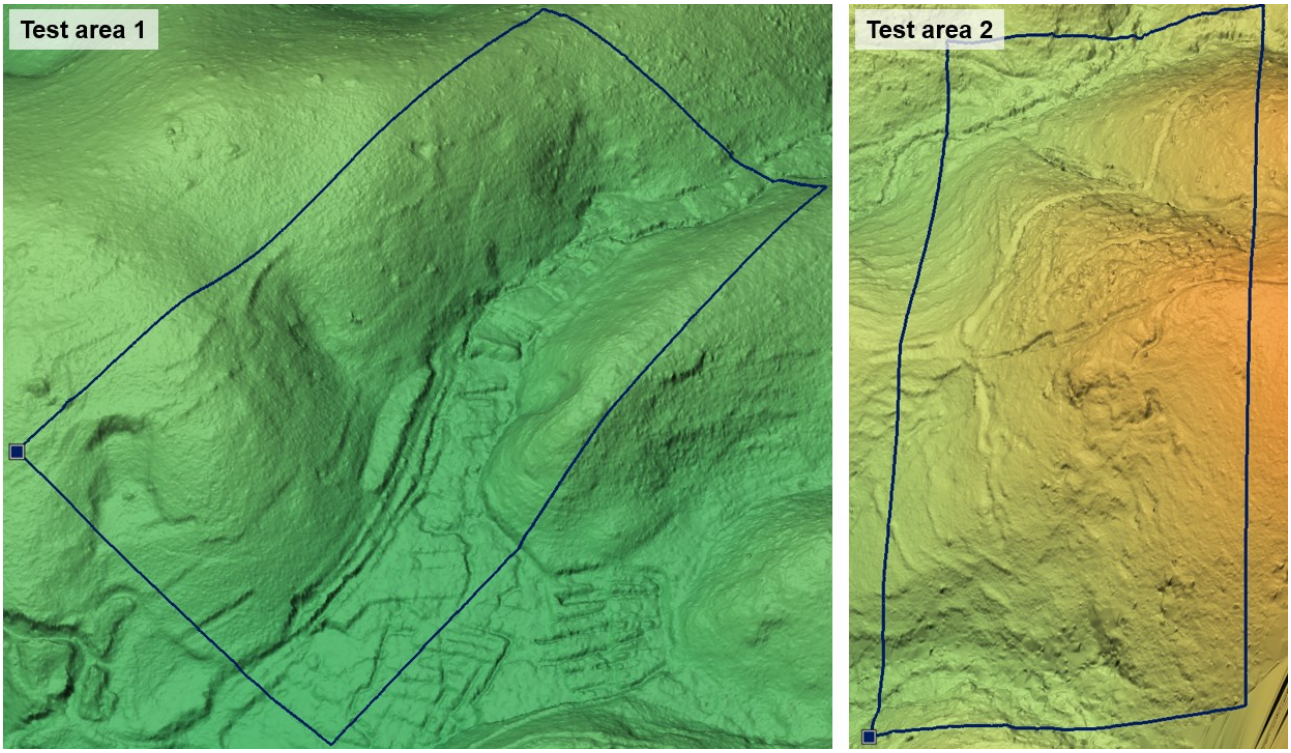

Fig. 9. 3D views generated by planlauf/TERRAIN based on the XYZ-DTM (© Irmela Herzog).

An alternative low-cost program (non-commercial licence) for DTM visualisations is planlauf/TERRAIN (planlauf GmbH, 2019). This Windows application uses gaming approaches for mesh decimation and thus allows virtual flights through the 3D landscape in real time that can be saved as mpeg files. The 3D environment provides a very intuitive approach for assessing the shape of a feature, thus supporting the decision if a feature is manmade (see also Verhoeven, 2017). The program includes many additional functions such as the import of shape files, marking features detected in the DTM by pins and exporting these pin locations in a CSV file. In Fig. 9, the outlines of the test areas were imported and high-resolution screenshots saved to file. It took some time to learn how to successfully invoke the functions listed above, but there are many more, which might prove useful. For instance, the two dimensional top views of the terrain may be exported in GeoTiff format for further processing in a GIS.

Analysis beyond visualisation

A cross-sectional view of the DTM allows checking if the structures identified in a visualisation are relevant or mere optical illusions. Based on such views, measuring the depth of depressions and the height of earth deposits is easy. Fig. 10 shows three cross sections for both SCOP++ DTMs. The locations of the vertical cut planes are indicated by the arrows in the maps. The cross section for the probable kiln location in the northeast of test area 1 clearly shows the differences between the two SCOP++ DTMs: the strategy 2 DTM is more smoothed, whereas more pronounced features but also spikes are visible in the strategy 1 DTM cross sections. Detecting such a depression with a depth of only about 35 cm but a width of 10 m in densely vegetated areas by walking is not possible. The depression in the east of test area 1 is more pronounced (about 2 m), and only minor differences between the two strategies are visible along this line (second cross section in Fig. 10). At the bottom

of Fig. 10, a cross section of a feature in the south of test area 2 is shown. The hill-shading visualisations suggested some similarity with a kiln-shaped depression, but the cross-section reveals that the shape is different.

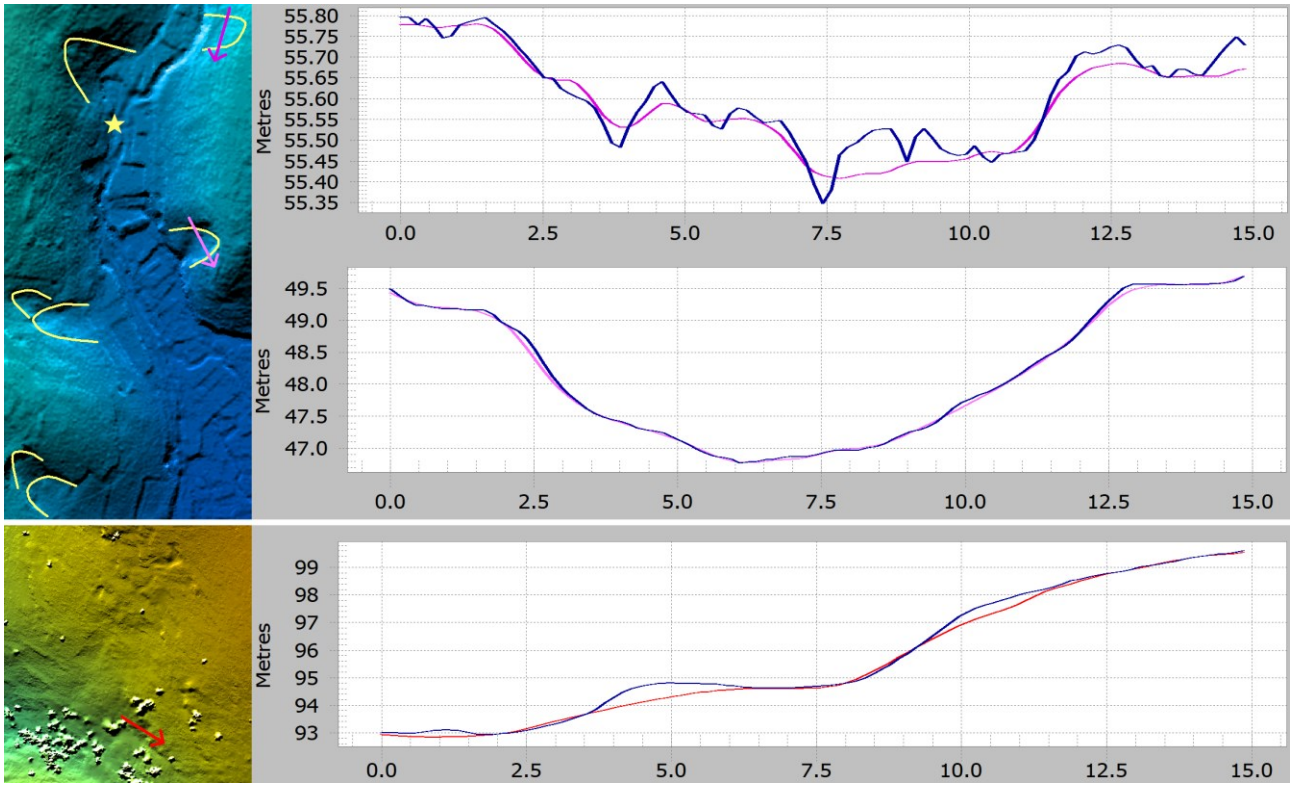

Fig. 10. Three cross sections (see maps on the left) of the SCOP++ DTMs: blue – strategy 1; violet/red – strategy 2 (© Irmela Herzog).

Most GIS software packages include a procedure for generating contour lines from a DTM. The archaeologists checking the kiln site candidates in the field reported that contour line maps (with labels) assist orientation in case of GPS inaccuracies. Contour lines were created with elevation intervals of 20 and 50 cm (Fig. 11 left: 50 cm).

Slope maps support delimiting manmade terraces, identifying platforms, and nearly level paths along a contour line (Doneus and Briese, 2006). The slope maps shown in Fig. 11 (centre and right) were generated by MIP/VM. Different methods for deriving slope from a DTM grid are implemented in GIS software, therefore the results might differ (de Smith et al., 2007, pp. 259–261). Future research with the aim of predictive modelling of Sue kiln sites will also apply slope maps: currently, it is assumed that the kilns are located on slopes ranging from 28 to 45 %. For this reason, this slope range is highlighted in yellow in Fig. 11 (centre and right). The probable kiln in the east of test area 1 (cf. Fig. 4a) is mostly steeper than this slope range, and this is one of the reasons why further investigations in the field are required. Moreover, slope maps also assist in identifying isolated misclassified points that appear as spikes in the DTM. The slope map typically displays very steep slopes in a small zone centred on these points (e.g. Fig. 11 right, southern part).

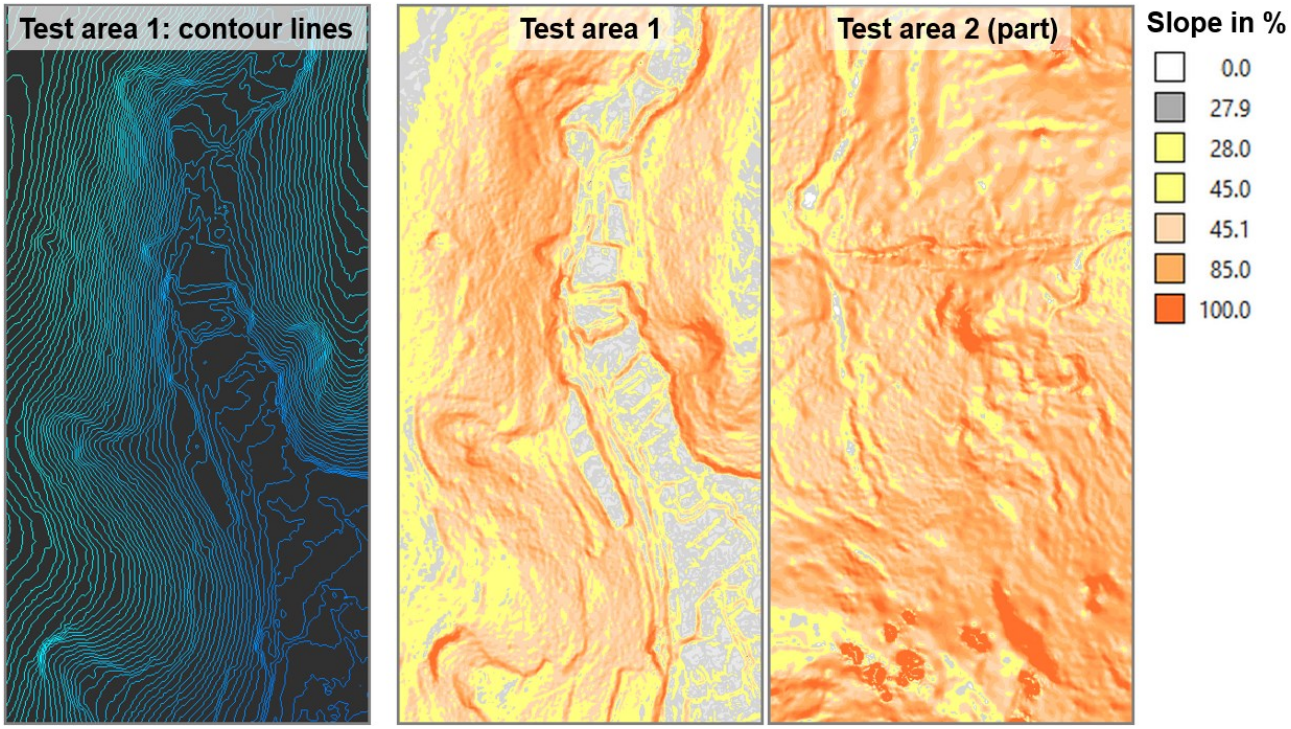

Fig. 11. Results of GIS methods: contour lines and slope maps (© Irmela Herzog).

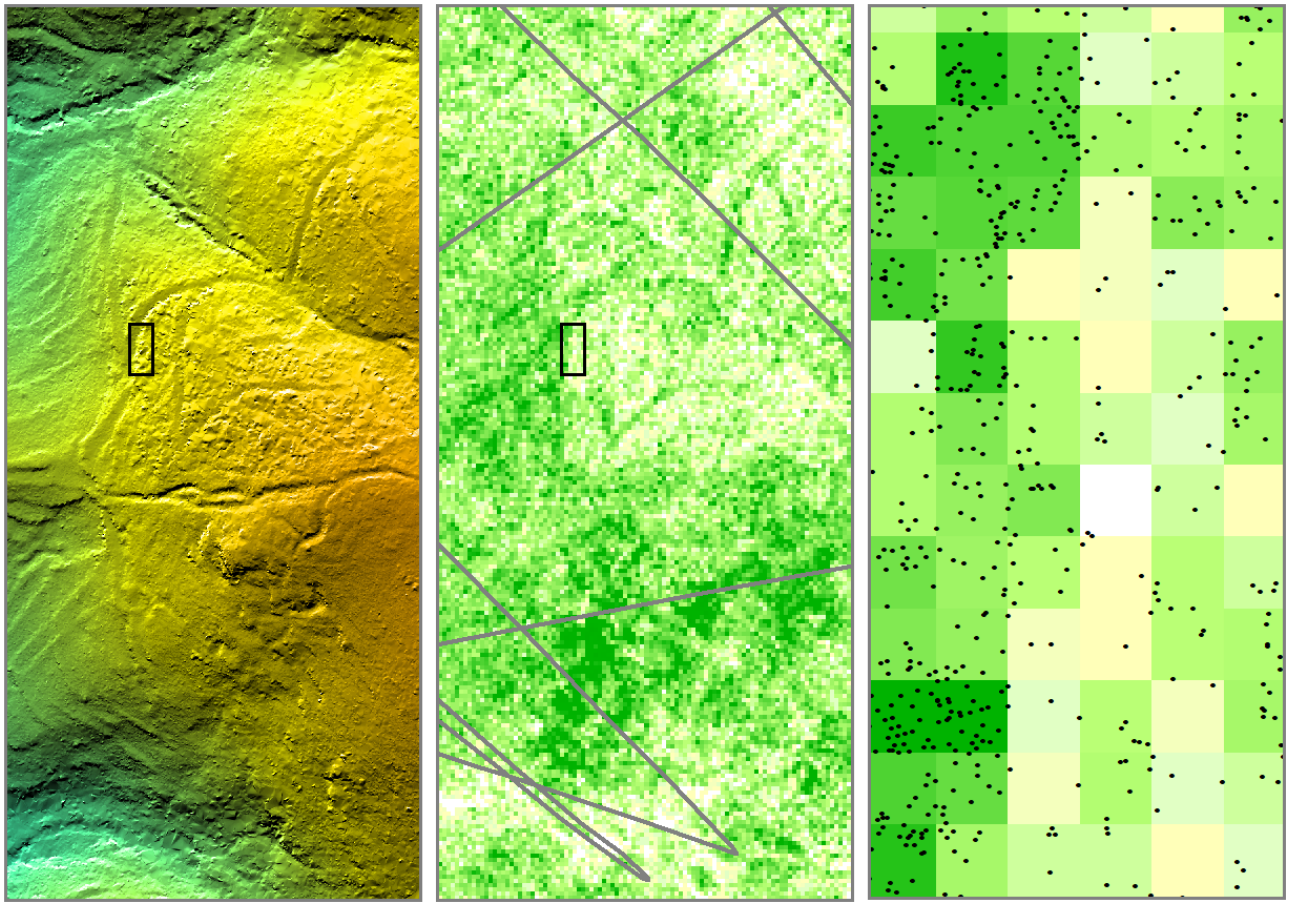

Fig. 12. Test area 2. Centre: Density map of the number of ground points in the XYZ files. Pixel size: 1 m².
Right: Enlargement of the area delimited by the black rectangle in the left and the centre image (© Irmela Herzog).

Simple approaches for assessing the reliability include a density map of the recorded surface points. Kernel density estimation with a bounded radial-symmetric Epanechnikov kernel (radius 1 m) was applied for generating a density map with a cell size of 1 m based on the XYZ points (de Smith et al., 2007, pp. 128–133). Fig. 12 illustrates the considerable variation in ground point density, showing the selected ground points in the image on the right. Although at least 100 points/m² were recorded, the filtering process sometimes selected only one of these points.

The DTM grid resolution does not necessarily correspond to the point density. According to the *Nyquist Limit*, also known as *Shannon's Sampling Theorem* (Beex, 2004), at least 1 point/m² must be present for reliable identification of an approximately rectangular archaeological feature with a minimum edge length of 2 m or more, i.e., the probable dimensions of the Sue kiln remains to be detected. So for instance in several patches located in the southern part of test area 2, it might not be possible to detect typical kiln sites reliably based on the XYZ data, even in the absence of ground point misclassifications. This area is well covered by UAV itineraries (grey lines in Fig. 12, centre). In some other parts of the survey area, the ground point density and the distance to the next UAV itinerary seems to be related. This observation, too, needs further investigation.

Discussion and conclusions

In the densely vegetated test region in south Japan with substantial variation of altitudes, UAV-based Lidar proved to be a viable survey method. Currently, reliability of ALS data in such complex situations is still an issue. Nevertheless, the two filter approaches presented—one of them tweaked for high detail, the other one minimising misclassifications of non-ground points in very densely vegetated areas—provide the basis for a large set of useful visualisations allowing to detect possible Sue kiln locations.

Free or low-cost software supports the creation of a large number of (archaeologically) useful visualisations. In this case study, SLRM, shaded relief from multiple directions and a combination of hillshade, slope and colour-coded heights seemed to be most helpful. Virtual cross sections are useful for validating the features recognized and assessing their depth or height. Validation should also include inspection of the ground point density in the areas considered. Slope maps allow delimiting former rice terraces, identifying platforms, and contour line paths.

In early spring 2019, field work aimed at checking 12 selected probable kiln sites identified in Lidar visualisations ruled out two of these locations, archaeological evidence for the existence of kilns in the other places was recorded (Shinoto et al., 2019a; 2019b). Supplemental magnetometer investigations at these locations are planned in near future. Orientation during ground inspection was assisted by SLRM maps and simple labelled contour maps (interval: 20 cm) in case of GPS inaccuracies. Additional ground-based archaeological investigations are planned for winter 2020/2021 with the aim of checking those probable kiln locations identified in the Lidar data that were not visited in spring 2019.

Unfortunately, the range of shapes of such kiln remains as well as their location parameters is not yet known for sure. Only after reliably identifying a large number of kiln sites, dependable predictive modelling and machine learning algorithms for detecting these archaeological features automatically in ALS data can be developed.

Acknowledgements

We greatly appreciate the suggestions, recommendations, and support by Baoquan Song, Michael Schmauder, Ute Knipprath, and Martin Schaich. Part of the project was funded by the Japan Society for the Promotion of Science (Class A, No. 15H01902, project leader N. Nakamura).

References

Akashi, Y. (2010). 'Landscapes of Ancient Mountain Fortresses – Viewing a Model from Digital Elevation Maps', *Chizu Chūshin*, 453, pp. 7–15 (in Japanese).

Beex, W. (2004). 'Use and Abuse of Digital Terrain Models', in Magistrat der Stadt Wien, Referat Kulturelles Erbe, Stadtarchäologie Wien (eds.) *Enter the Past. The E-way into the Four Dimensions of Cultural Heritage. CAA 2003, Computer Applications and Quantitative Methods in Archaeology, Proceedings of the 31st Conference,* Vienna, Austria, April 2003. *BAR International Series,* 1227: Oxford, pp. 240–242.

de Smith, M.J., Goodchild, M. and Longley, P.A. (2007). *Geospatial Analysis: A Comprehensive Guide to Principles, Techniques and Software Tools*. Leicester: Matador.

Doneus, M. and Briese, C. (2006). 'Digital terrain modelling for archaeological interpretation within forested areas using full-waveform laserscanning', in M. Ioannides, D. Arnold, F. Niccolucci and K. Mania (eds.), *The 7th International Symposium on Virtual Reality, Archaeology and Cultural Heritage VAST*, pp. 155–162.

Doneus, M., Mandlburger, and G., Doneus, N. (2020). Archaeological filtering of airborne laser scan derived point-clouds in difficult environments, *Journal of Computer Applications in Archaeology,* 3(2), pp. 92–108. doi: 10.5334/jcaa.44.

Hesse, R. (2010). 'LiDAR-derived Local Relief Models: a new tool for archaeological prospection', *Archaeological Prospection*, 17(2), pp. 67–72. doi: 10.1002/arp.374.

Hesse, R. (2016). 'Visualisierung hochauflösender Digitaler Geländemodelle mit LiVT', in Lieberwirth, U. and Herzog, I. (eds.), *3D-Anwendungen in der Archäologie*. Computeranwendungen und Quantitative Methoden in der Archäologie. Workshop der AG CAA und des Exzellenzclusters TOPOI 2013. *Berlin Studies of the Ancient World,* 34, pp. 109–128.

Herzog, I. (2017). 'Reconstructing Pre-Industrial Long Distance Roads in a Hilly Region in Germany, Based on Historical and Archaeological Data', *Studies in Digital Heritage*, 1(2), pp. 642–660. doi: 10.14434/sdh.v1i2.23283.

Kokalj, Ž., Zakšek, K., and Oštir, K. (2013). 'Visualizations of lidar derived relief models', in Opitz, R. and Cowley, C.D. (eds.) *Interpreting Archaeological Topography—Airborne Laser Scanning, Aerial Photographs and Ground Observation*. Oxford: Oxbow Books, pp. 100–114.

Kokalj, Ž. and Somrak, M. (2019). Why Not a Single Image? Combining Visualizations to Facilitate Fieldwork and On-Screen Mapping. *Remote Sensing,* 11(7), article no. 747.

Matsusaki, H. (2018). 'Distribution Survey in the Ancient Nakadake Kiln Site Cluster', *The Journal of the Archaeological Society of Kyushu*, 93, pp. 133–142 (in Japanese).

Nakamura, N. and Shinoto, M. (2015). 'Summary of the excavation and related research on a Sue ware kiln site cluster in Nakadake Sanroku, South Japan, 2013–2015', in Nakamura, N. and Shinoto, M. (eds.), Studies on the Nakadake Kiln Site Cluster, pp. 121–122 (in English). Available at http://hdl.handle.net/10232/23138 (Accessed: 02 May 2020).

Nakamura, N. and Yoshimoto, M. (2015). 'I The excavation in the kiln site cluster at Nakadake Sanroku', in Nakamura, N. and Shinoto, M. (eds.), *Studies on the Nakadake Kiln Site Cluster*, pp. 1–48 (in Japanese). Available at http://hdl.handle.net/10232/23138 (Accessed: 02 May 2020).

planlauf GmbH (2019). planlauf/TERRAIN (Version 2018 R2) [Computer program]. Available at: https://planlaufterrain.com/ (Accessed: 29 June 2019).

Pfeifer, N., Stadler, P., and Briese, C. (2001). Derivation of digital terrain models in the SCOP++ environment. In Proceedings of OEEPE Workshop on Airborne Laserscanning and Inferometric SAR for Detailed Digital Terrain Models, OEEPE (ed.): Stockholm, Sweden.

Shinoto, M. and Nakamura, N. (2016). 'Nakadake: Forschungen in einem japanischen Töpferzentrum', *Blickpunkt Archäologie*, 2016(4), pp. 298–307.

Shinoto, M., Ōnishi, T., Herzog, I., Doneus, M., Song, B., Nakamura, N., Haijima, H., and Kita'ichi, S. (2019a). 'Detecting Sue kilns with LiDAR technology: Visualizations and results from the kiln site cluster in Nakadake Sanroku, Kagoshima Prefecture', *The 36th Annual Meeting of the Japan Society for Scientific Studies on Cultural Property. Abstracts*, pp. 96–97 (in Japanese).

Shinoto, M., Herzog, I., Doneus, M., Haijima, H., Song, B., Ōnishi, T., Nakamura, N., and Kita'ichi, S. (2019b). 'Identifying archaeological sites from elevation data: LiDAR data analysis in a densely forested mountainous area', *The 36th Annual Meeting of the Japan Society for Scientific Studies on Cultural Property. Abstracts*, pp. 290–291 (in Japanese).

Verhoeven, G.J.J. (2017). 'Mesh Is More—Using All Geometric Dimensions for the Archaeological Analysis and Interpretative Mapping of 3D Surfaces', *Journal of Archaeological Method and Theory*, 24(4), pp. 999–1033. doi: 10.1007/s10816-016-9305-z.